A Restoration and Extrapolation Iterative Method for Band-limited Fluorescence Microscopy Image

Moacir P. Ponti-Junior[1], Nelson D. A. Mascarenhas[1], Cláudio A. T. Suazo[2]
[1]Departamento de Computação – Universidade Federal de São Carlos, São Carlos, SP, Brasil.
[2]Departamento de Engenharia Química – Universidade Federal de São Carlos, São Carlos, SP, Brasil.
moacir@dc.ufscar.br, nelson@dc.ufscar.br, claudio@power.ufscar.br

Abstract

Optical microscopic images, especially with a nonconfocal microscope, are fundamentally limited because the optical transfer function (the Fourier transform of the point-spread function) is zero over a region of the spatial-frequency domain. Iterative algorithms were developed for the restoration and extrapolation of diffraction-limited imagery. In this paper we present the effectiveness of an iterative method based on the Richardson-Lucy algorithm for image restoration and a simultaneous modified version of Gerchberg-Papoulis method to extrapolate the spectrum and control the noise amplification. Good convergence stabilization results were achieved and also good numerical results were observed.

1. Introduction

Like the human eye, most instruments cannot discern fine details. Microscopic images are often used on medical and biological research and are severely affected by blurring due to the limited size of the aperture lens. Since the formation of an image alters the recorded information content from that of the original object, there is interest directed to processing images so that it closely matches the original object.

Fourier optics demonstrates that there exists a cut-off spatial frequency, which is directly determined by the shape and size of the limiting pupil in the optical system [1]. This distortion of the spatial frequency components is governed by the OTF (Optical Transfer Function), the normalized Fourier transform of the PSF (Point Spread Function) of an imaging system. The PSF describes the spatial spread for a single point input.

Credible methods appeared in the last decades for the reconstruction of spatial frequencies of the object within the diffraction limit [2]. For instance, Richardson and Lucy [3] [4] defined a probabilistic method to restore images which formation can be modeled by a Poisson process such as in telescopic and microscopic systems. However, the ability of restoration of frequencies beyond the image or signal passband are controversial with literature proclaiming it as not possible [2] [5].

After the work of Pollak, Landau and Slepian [6] that used prolate spheroidal functions, Gerchberg and Papoulis [7] [8], showed that the imposition of known constraints on frequency and time domain could extrapolate a signal, but they do not present a good estimation of the original image, since they are not concerned with blur and noise. A blind deconvolution method that used constraints on space and frequency domain was also proposed [9]. In the middle of 1990's, Hunt [5] and Carrington [10] showed the possibility of superresolution through non-negativity and other constraints that used as *a priori* knowledge in the performed algorithms. Conchello [11] studied the band extrapolation capability of the Expectation-Maximization algorithm. A recent paper applied a mathematical extrapolation [12] with good results, but the method also assumed absence of noise. Sementilli et al. [13] showed other examples of recovering information from beyond the diffraction limit. A previous work [14] also used a non-linear filter to achieve extrapolation.

This work proposes a restoration method that simultaneously can restore frequencies within the diffraction limit and also enhance the spectrum beyond this limit for fluorescence microscopy images. These images are band-limited and modeled by photon statistics, so they have implicit Poisson noise that could difficult the convergence, as will be described in next section.

The unification of restoration, denoising and extrapolation in one algorithm is a goal we are pursuing and the paper shows the possibility of that unification. The approach used was to carry out a joint use of a Gerchberg-Papoulis iteration, together with a median filter, and an Richardson-Lucy step to restore frequencies and control the noise. This is the main

1530-1834/07 $25.00 © 2007 IEEE
DOI 10.1109/SIBGRAPI.2007.25

contribution of this work, which shows the possibility of classical algorithms improvement solving old convergence problems that appear in problems like going beyond the diffraction limit in the presence of noise.

2. Fluorescence Microscopy Images

The general imaging system for an optic wide-field microscope has two main stages as shown on Figure 1. The first stage is a lens system that causes the blurring. Due to the photon counting nature of light based sensors, the noise can be modeled by a Poisson distribution. Then, a CCD camera is used to acquire and to quantize the image.

The microscopy images of the present work were acquired on a scientific wide-field microscope with a CCD camera attached. The images were obtained under a low exposure to avoid photobleaching, a process that causes loss of fluorescence [15]; therefore it generates a signal dependent noise that can be modeled by a Poisson distribution. There is another kind of noise added to the image due to the CCD electronic device, often modeled by a Gaussian distribution [16].

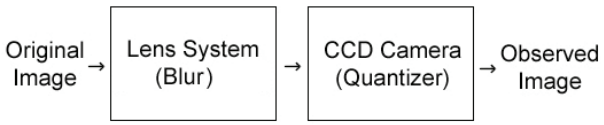

Figure 1. Stages of microscopy imaging system

The image formation can be modeled as:

$$g(x,y) = h(x,y) * f(x,y) + n(x,y), \qquad (1)$$

where g is the observed image, h the point spread function (PSF) that models the blurring due to the optical system, f is the original image, * is a two-dimensional convolution operator and n is the additive Gaussian noise - the electronic CCD adds Gaussian noise but it is not significant compared to the Poisson photon counting noise [16].

Since the convolution is a computational expensive procedure, we use the convolution theorem of Fourier Transform to use a simple product:

$$G(u,v) = H(u,v) \cdot F(u,v) + N(u,v), \qquad (2)$$

where the capital letters indicates the Fourier transform of each object described on equation 1. The model described is suitable for an incoherent imaging system [1].

The natural solution would be the inverse filter:

$$F(u,v) = \frac{G(u,v)}{H(u,v)} + \frac{N(u,v)}{H(u,v)}. \qquad (3)$$

Unfortunately, practical OTF have zero valued regions (beyond the diffraction limit), resulting in no information on these areas, and low valued regions that can amplify the noise. Also, it does not model the Poisson process nature of the microscopy system.

3. Richardson-Lucy Deconvolution Method

The Richardson-Lucy (RL) algorithm [3] [4] uses a probabilistic approach.

In fluorescence microscopy, the recorded image can be viewed as a Poisson process. Suppose the noise is white, the probability is:

$$p(g \mid \hat{f}) = \prod_{\mathbf{x}} \left(\frac{h(\mathbf{x}) * \hat{f}(\mathbf{x})^{g(\mathbf{x})} e^{-h(\mathbf{x}) * \hat{f}(\mathbf{x})}}{g(\mathbf{x})!} \right), \quad (4)$$

where **x** represents the (x,y) pair for a 2D signal.

The non-regularized RL algorithm minimizes the functional $-\log p(g \mid \hat{f}) = J_1(\hat{f})$, giving the maximum likelihood estimation:

$$J_1(\hat{f}) = \sum_{\mathbf{x}} \begin{pmatrix} -g(\mathbf{x}) \cdot \log[(h * \hat{f})(\mathbf{x})] + \\ + (h * \hat{f})(\mathbf{x}) \end{pmatrix}. \qquad (5)$$

The RL iteration is given by:

$$\hat{f}_{n+1}(\mathbf{x}) = \left[\left(\frac{g(\mathbf{x})}{\hat{f}_n(\mathbf{x}) * h(\mathbf{x})} \right) * h(-\mathbf{x}) \right] \cdot \hat{f}_n(\mathbf{x}). \quad (6)$$

This extensively used algorithm is generally stopped at a finite number of iterations. In real situations, the deconvolution is an ill-posed problem, so the RL iterations result in only noise when the number of iterations $n \to \infty$. The level of noise in fluorescence microscopy is often high so regularization methods are used in order to minimize the undesirable effects.

4. Filtered Gerchberg-Papoulis

The Gerchberg-Papoulis (GP) algorithm [7] [8] assumes that there is some knowledge about the bandwidth and iteratively imposes the requirements that the signal is band-limited and matches the known portion of the signal.

Let $g(\mathbf{x})$ have a spectrum $G(\mathbf{u})$ and Ω the region where $G(\mathbf{u})$ is nonzero. Since $g(\mathbf{x})$ is known within a region *T*, the aperture is defined by:

$$B_T = \begin{cases} 1, & (\mathbf{x}) \in T \\ 0, & (\mathbf{x}) \notin T. \end{cases} \quad (7)$$

The spectral pupil is defined as:

$$B_\Omega = \begin{cases} 1, & (\mathbf{u}) \in \Omega \\ 0, & (\mathbf{u}) \notin \Omega. \end{cases} . \quad (8)$$

So, the algorithm consists on:

$$\hat{e}_0(\mathbf{x}) = B_T g(\mathbf{x}), \quad (9)$$

$$\hat{e}_{n+1}(\mathbf{x}) = B_T g(\mathbf{x}) + (1 - B_T) \cdot L_\Omega \hat{e}_n(\mathbf{x}), \quad (10)$$

Where $\hat{e}_0(\mathbf{x})$ is the first estimation of the extrapolated image, $\hat{e}_{n+1}(\mathbf{x})$ is the estimation at iteration *n+1*, and $L_\Omega = \Im^{-1} B_\Omega \Im$ is the frequency domain constraint operator. The convergence proof of this method can be found in [7] [8].

The convergence of this method assumes absence of noise. So, the algorithm was modified in order that it could deal with noise. For each iteration, the magnitude of the extrapolated frequencies, found beyond the limit Ω, is filtered by a median filter.

Since the frequency extrapolation, rather than spatial extrapolation, is the goal of this work, the iteration was changed to:

$$E'_{n+1}(\mathbf{u}) = (1 - B_\Omega) \cdot \mathrm{MF}\{E_n(\mathbf{u})\} + B_\Omega E_0(\mathbf{u}), \quad (12)$$

$$\hat{e}_{n+1}(\mathbf{x}) = B_T \Im^{-1}\{E'_{n+1}(\mathbf{u})\}, \quad (13)$$

where $E_n(\mathbf{u})$ is the Fourier transform of the previous estimation, MF is a function that apply the median filter in the magnitude of $E_n(\mathbf{u})$, $E_0(\mathbf{u})$ is the Fourier transform of the first estimation and the $\hat{e}_{n+1}(\mathbf{x})$ is the restored image at iteration *n+1*.

The modified algorithm constrains the spatial limit in order to extrapolate the frequency limit. The original method constrains the frequencies to extend the spatial limit.

The median filter was used due to the noise spatial characteristic when it is amplified by the restoration method. The resulting noise is similar to a salt-and-pepper noise. This noise behavior was observed in the experiments carried out which results are shown in section 7.

The idea of combining a GP step, together with a median filter, and an RL step is to restore frequencies within and beyond the diffraction limit with improvement in noise control.

5. Simultaneous Extrapolation-Restoration

The method proposed here simultaneously applies the RL algorithm and the filtered GP algorithm, as follows:

$$\hat{f}_{n+1}(\mathbf{x}) = RL[e_n(\mathbf{x})], \quad (14)$$

$$\hat{e}_{n+1}(\mathbf{x}) = FGP[\hat{f}_{n+1}(\mathbf{x})], \quad (15)$$

where RL is the Richardson-Lucy restoration method and FGP is the Filtered Gerchberg-Papoulis algorithm, modified in order to perform band extrapolation (instead of spatial extrapolation). A median filter was also added to the algorithm. The objective of the filter is to attenuate the noise amplification, since for real problems the algorithms result in only noise when the number of iterations $n \to \infty$.

The diagram in Figure 2 shows the algorithm flow. The algorithm starts with a RL iteration (1). The result of the iteration is transformed to frequency domain (2). The spectral pupil constraint is imposed on the original image (3), and the extrapolated spectrum obtained is added keeping the known signal (4). The image is transformed to the spatial domain (5) and the image is constrained in space (6). The result of the extrapolation step is used as a new estimation to the RL iteration (1) and so on.

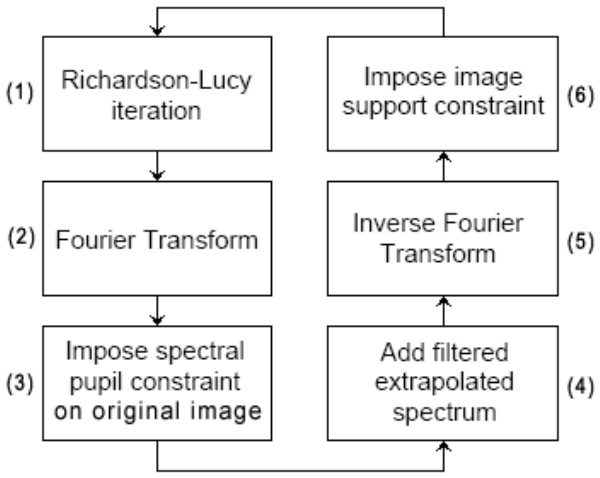

Figure 2. Algorithm diagram

The first estimation of the image is the same described in the Gerchberg-Papoulis method.

We expect to observe a smoother result in flat areas with a cost of loosing some sharpness on edge areas.

The algorithm stops in a determined number of iterations, since the algorithm convergence is not assured.

6. Experiments

A simulated experiment was carried out using a phantom image, with 256x256 pixels. This image was blurred by a Gaussian filter size [9x9] and $\sigma^2 = 16$. Poisson noise was also embedded to the image so that the distorted image yields a PSNR (Peak Signal-to-Noise Ratio) of 7.8dB. This phantom was built so that we could measure the image improvement using numerical evaluation methods. High contrast and flat areas were used to observe the behavior of noise and the restoration in edge areas. The original and degraded phantom images are shown in Figure 3.

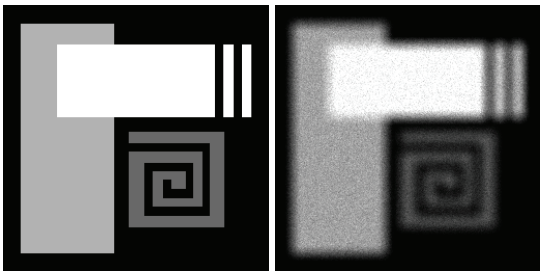

Figure 3. Original image (left); Distorted image (right)

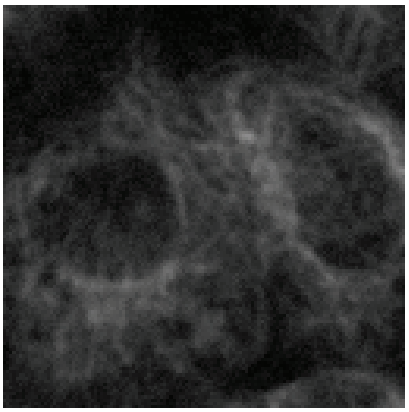

Figure 4. Fluorescence microscopy observed image

An image (Figure 4) obtained from a cell culture was also used to perform an experiment, in order to observe the behavior of the method with real images. Although it is impossible to measure the improvement after the restoration, a visual inspection and the spectral enhancement can be observed.

Three iterative methods were used to restore the images: (1) Richardson-Lucy; (2) Richardson-Lucy with Gerchberg-Papoulis; (3) Richardson-Lucy with Filtered Gerchberg-Papoulis.

6.1. Evaluation Methods

The results were evaluated by observing ISNR (Improvement on Signal-to-Noise Ratio) and the UIQI (Universal Image Quality Index) [17] concerning the phantom images.

The ISNR is given by:

$$ISNR = 10\log_{10}\left\{\frac{\sum_i [g(\mathbf{x}_i) - f(\mathbf{x}_i)]^2}{\sum_i [\hat{f}(\mathbf{x}_i) - f(\mathbf{x}_i)]^2}\right\}, \quad (16)$$

where $g(\mathbf{x})$ is the degraded image, $f(\mathbf{x})$ the original image and $\hat{f}(\mathbf{x})$ the restored image. The ISNR measures the differences at each pixel from degraded and restored images comparing with the original image and yielding a number proportional to the improvement on pixel similarity sense.

The UIQI is given by:

$$U = \frac{4\sigma_{xy}\overline{xy}}{(\sigma_x^2 + \sigma_y^2)[(\bar{x})^2 + (\bar{y})^2]}, \quad (17)$$

where $\bar{x}$, $\bar{y}$, σ_x^2 and σ_y^2 are the average and variance of the original (x) and restored (y) images, respectively, and σ_{xy} is the correlation coefficient between x and y. The dynamic range of U is [−1, 1]. The best value (1) is achieved if and only if $x = y$.

The UIQI is an alternative to the ISNR since it models the image distortion as a combination of loss of correlation, luminance distortion and contrast distortion, comparing the original and processed image. The loss of correlation is related to the band limit, so we expect to observe a higher UIQI for extrapolated images.

The numerical evaluation methods presented here cannot be applied to the real image, since the original image is not available. To evaluate the restoration/extrapolation of the real image, the autocorrelation coefficients, which indicate high

frequency enhancement, were plotted to observe the spectrum spread. The restored images were also included to observe the visual quality improvement.

7. Results

The degraded phantom image was restored using the three algorithms as described in section 5. The ISNR and UIQI results obtained with each method are shown in Table 1 for 5 and 30 iterations.

Figure 5 shows the degraded image and the restored images using 30 iterations. The smoothness of the result on flat areas can be observed with use of the proposed method.

Figure 6 and 7 shows the ISNR values in terms of the iterations. It is interesting to observe in this figure the behavior of the ISNR during the restoration process. The ISNR drops very sharply with the use of RL algorithm without regularization and constraints. Using the proposed algorithm based on the filtered GP method, the imposition of the filtered estimated part of the signal can stop the noise amplification and help the restoration algorithm to stabilize the result.

The real image restoration is shown in the Figure 8 (using RL method) and Figure 9 (using RL with filtered GP method). The image restored with the proposed method is visually better. The plotting of autocorrelation coefficients is shown in Figure 10. The decay of autocorrelation coefficients curve indicates the enhancement of the spectrum. The curve decrease faster for high frequency enhancement. It is possible to see the good results obtained and also a better stability while iterations increase.

Another interesting point is that the noise changes within the iterations and "inverted peaks" are observed in flat areas. For instance "black peaks" can be observed on the white flat area in the RL restoration (Figure 5 top right). Since it is similar to a salt-and-pepper noise, the median filter was used instead of others that would just smooth the artifacts.

Table 1. Restoration results

Image	ISNR	UIQI
Degraded Image	-	0.18
Results with 5 iterations		
Richardson-Lucy	0.81	0.28
Richardson-Lucy with GP	0.92	0.14
Richardson-Lucy with Filtered GP	**1.04**	**0.30**
Results with 30 iterations		
Richardson-Lucy	-1.23	0.09
Richardson-Lucy with GP	0.12	0.10
Richardson-Lucy with Filtered GP	**0.38**	**0.29**

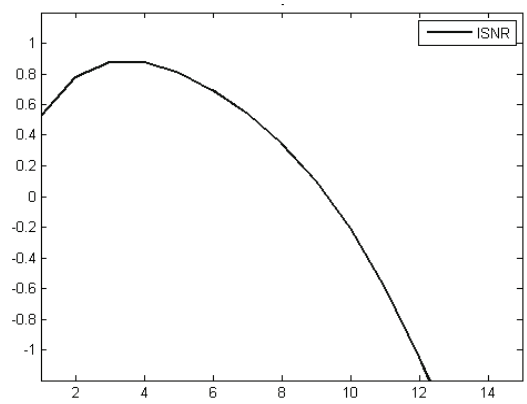

Figure 6. ISNR for RL iterations

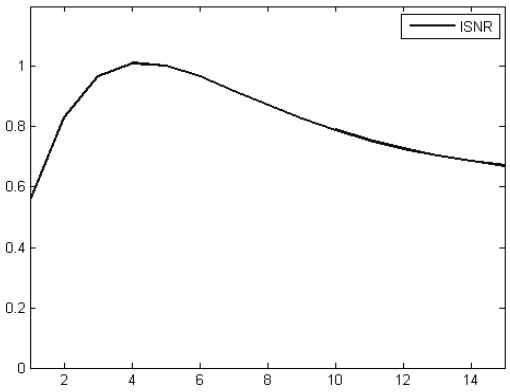

Figure 7. ISNR for RL with filtered GP iterations

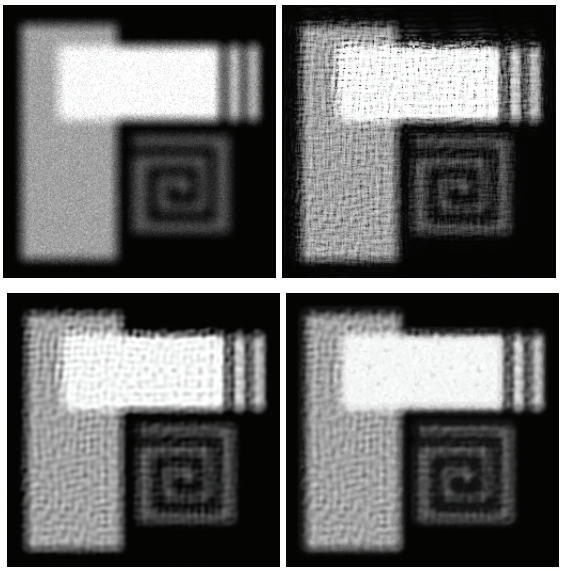
Figure 5. Degraded image (top left); Restored images with 30 iterations: RL (top right); RL-GP (bottom left); and RL with filtered GP (bottom right)

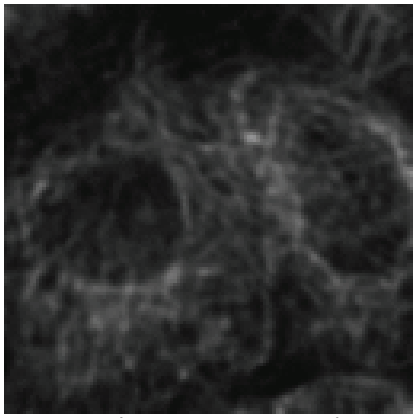

Figure 8. Restored image using RL with 30 iterations

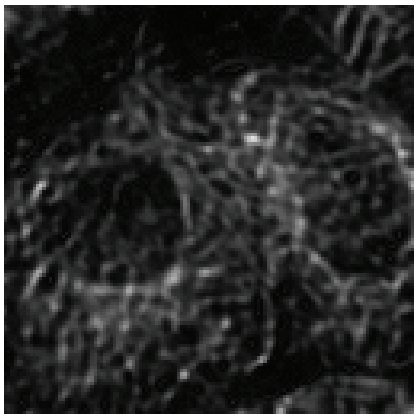

Figure 9. Restored image using RL with filtered GP with 30 iterations

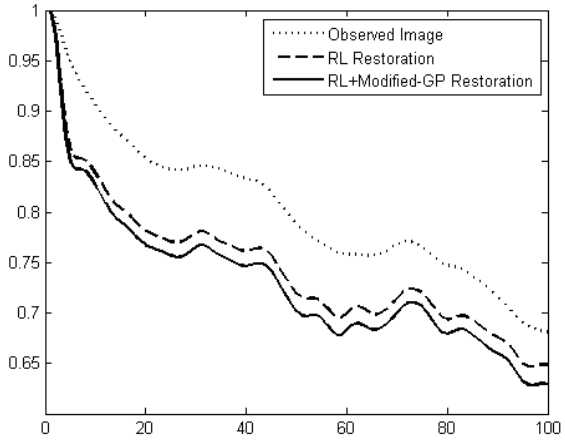

Figure 10. Autocorrelation coefficients (dot line: original image; dashed line: RL; solid line: RL-Modified GP)

8. Conclusions

The presence of noise is always a difficult problem to overcome. The majority of methods are very efficient just in absence of noise. In fact, some of methods do not have a convergence proof and when there is, the signal is assumed to be noise-free [4] [7] [12] [13].

A modified approach of the Gerchberg-Papoulis was used simultaneously with the Richardson-Lucy deconvolution to deal with noise. The idea of the algorithm was to restore frequencies within the passband (with use of the RL method), and also beyond it, filtering the results to avoid noise amplification.

Good results on ISNR and UIQI index were observed, and also a faster autocorrelation coefficients curve decrease, indicating spectral extrapolation. The proposed method was able to restore frequencies and also contain the noise amplification, performing band extrapolation.

New advances could study the behavior of noise while the iterations increase. Also, a future work could apply more accurate filters to deal with the noise without a loss of sharpness in details. New spatial and frequency constraints could also improve the image quality and achieve a better extrapolation.

9. Acknowledgment

We would like to thank the Animal Cell Laboratory of the Chemical Engineering Department for providing the images used in this work, especially Kamilla Swiech and Bruna Silva. This work was also partially supported by a CAPES Brazilian student scholarship and FAPESP-Brazil Thematic Project 02/07153-2.

10. References

[1] Goodman, J.W., *Introduction to Fourier Optics*, 2.ed, McGraw Hill, 1996.

[2] Andrews, H.C., and Hunt B.R., *Digital Image Restoration*, Prentice-Hall, 1977.

[3] W.H. Richardson. "Bayesian-Based Iterative Method of Image Restoration". *Journal of Optical Society of America*, v.62, n.1, 1972, pp. 55-59.

[4] L.B. Lucy. "An Iterative Technique for the Rectification of Observed Distributions". *The Astronomical Journal,* v.79, n.6, 1974, pp. 745-765.

[5] B.R. Hunt, "Super-Resolution of Images: Algorithms, Principles, Performance", *International Journal of Imaging Systems and Technology*, v.6, 1995, pp. 297-304.

[6] Jansson, P.A.. *Deconvolution of Images and Spectra*. Academic, 1997.

[7] R.W. Gerchberg, "Super-resolution Through Error Energy Reduction" *Opt. Acta*, v.21, 1974, pp. 709-720.

[8] A. Papoulis, "A New Algorithm in Spectral Analysis and Band-Limited Extrapolation", *IEEE Trans. Circuits and Systems*, v.22, n.9, 1975, pp. 735-742.

[9] G.R. Ayers, and J.C. Dainty. "Iterative Blind Deconvolution Method and its Applications". *Optics Letters*. v.13, n.7, 1988, pp 547-549.

[10] W.A. Carrington, R.M. Lynch, E.M. Moore, G. Isenberg, K.E. Fogarty, and F.S. Fay, "Superresolution Three-Dimensional Images of Fluorescence in Cells with Minimal Light Exposure". *Science,* v. 268, 1995, pp. 1483-1487.

[11] J.A. Conchello, "Superresolution and Convergence Properties of the Expectation-Maximization Algorithm for Maximum-Likelihood Deconvolution of Incoherent Images". *Journal of Optical Society of America A*, v.15, n.10, 1998, pp. 2609-2619.

[12] S. Bhattarcharjee, M.K. Sundareshan, "Mathematical Extrapolation of Image Spectrum for Constraint-Set Design and Set-Theoretic Superresolution. *Journal of Optical Society of America A,* v.20, n.8, 2003, pp. 1516-1527.

[13] P. Sementilli P., B. Hunt, and M. Nadar, "Analysis of the Limit to Super-resolution in Incoherent Imaging". *Journal of Optical Society of America A*, v.10, 1993, pp. 2265-2276.

[14] H. Greenspan, C.H. Anderson, S. Akber, "Image Enhancement by Nonlinear Extrapolation in Frequency Space". *IEEE Transactions on Image Processing*, v.9, n.6, 2000, pp. 1035-1048.

[15] L. Song, E.J. Hennink, I.T. Young, H.J. Tanke. "Photobleaching Kinetics of Fluorescein in Quantitative Fluorescence Microscopy". *Biophysical Journal*, v.68, 1995, pp. 2588-2600.

[16] L.J. van Vliet, F.R. Boddeke, D. Sudar, and I.T. Young, "Image Detectors for Digital Image Microscopy", in: M.H.F. Wilkinson, F. Schut (eds.), Digital Image Analysis of Microbes; Imaging, Morphometry, Fluorometry and Motility Techniques and Applications, Modern Microbiological Methods, John Wiley & Sons, 1998, pp. 37-64.

[17] Wang, Z., Bovik, A.C. "A Universal Image Quality Index". *IEEE Signal Processing Letters*, v.9, n. 3, 2002. pp.81-84.